A Bidirectional Deep-Learning Algorithm to Forecast Regional Ionospheric TEC Maps

Kondaveeti Sivakrishna, Devanaboyina Venkata Ratnam, *Senior Member, IEEE*, and Gampala Sivavaraprasad, *Member, IEEE*

***Abstract*—The rapid evolutions in artificial intelligence and the machine learning era have significantly improved accuracy for ionospheric space weather forecasting models. The ionospheric total electron content (TEC) forecasting is necessary to alert global navigation satellite system (GNSS) users about ionospheric space weather influences on satellite-receiver radio communications. Precise modeling and forecasting of the ionospheric TEC are critical for reliable and accurate GNSS applications. In this article, a deep-learning-based bidirectional long short-term memory (bi-LSTM) algorithm is implemented for 26 global positioning system stations TEC data over the Indian region. The bi-LSTM ionospheric TEC forecasting maps are generated and compared with ANN and LSTM models during both geomagnetic quiet and disturbed periods. The potential of bi-LSTM networks in time-sequence processing is improved by having forward and backward connections. The bi-LSTM results are demonstrated with and without solar and geomagnetic indices as input to the network. This work's outcome would help to develop an ionospheric weather alert system for GNSS users.**

***Index Terms*—Adjusted spherical harmonics function (ASHF), artificial intelligence (AI), bidirectional long short-term memory (bi-LSTM), deep learning (DL), forecast, global positioning system (GPS), ionosphere total electron content (TEC).**

I. Introduction

THE forecasting of spatial and temporal ionospheric total electron content (TEC) variations is challenging, especially over the low-latitude regions due to the complex behavior of the ionosphere ascribed to EIA [1]. The low-latitude ionospheric behavior is complex and influences the forecasting accuracy of models. Global positioning system (GPS) measurements are crucial and most useful for monitoring the ionosphere and predicting the TEC variations [2]. The long-term vertical TEC (VTEC) data derived from GPS measurements provide an opportunity to understand the ionospheric behavior and develop ionospheric TEC forecasting models. The Indian low-latitude GPS network of 26 GPS receivers as a part of the geoaugmented navigation system is operational for civil aviation, navigation, and timing applications.

Krishna *et al.* [3] have implemented a regional adjusted spherical harmonics function (ASHF) based TEC model using 26 GPS TEC stations data over the Indian region. The ASHF TEC model performed well to capture northern EIA features and ionospheric TEC variability for quiet and disturbed day conditions [3]. These ionospheric TEC time-series forecasting models are implemented at a specific location using time series and statistical methods [4]–[6]. The machine learning (ML) techniques successfully forecast ionospheric TEC variability. The ML techniques, such as multilayer feedforward networks and long short-term memory (LSTM) networks, are implemented to specify the ionospheric TEC patterns by approximating the relation between the observed ionospheric parameters and geophysical conditions solar activities, latitude/longitude, local time, and seasons [7].

The deep-learning (DL) technique based on conditional generative adversarial networks is used to forecast global TEC maps one-day ahead [8]. Saed *et al.* have proposed a solar flare predictions model using the ML technique, the support vector machine (SVM) model with center for orbit determination in Europe global ionospheric TEC maps (GIM) TEC data. The SVM method is implemented for classifying daily, temporal, and spatial TEC changes before solar flare events, such as B-, C-, M-, and X-class [9]. The extreme gradient boosting over decision trees model is developed to generate TEC maps by a set of regression estimations [10].

ML techniques are also applied using local global navigation satellite system (GNSS) stations to obtain regional ionospheric predictions [11], [12]. A DL recurrent neural networks (RNNs) are implemented for forecasting TEC at Beijing GPS station (40°N, 115°E) [13]. The RNN networks are computationally more powerful than the feedforward networks due to their capability to incorporate past information based on the internal recurrence. However, these networks suffer from gradient vanishing and exploring problems. Therefore, it is difficult to train the network for learning the information based on the long-term TEC data. LSTM networks are the extension of RNN and learn the information for training long-period TEC time-series data to overcome the long-term problems of RNN [14]. Neural-network-based ionospheric TEC model and an extended encoder–decoder LSTM were established to forecast the ionospheric VTEC over China [15]. The LSTM for TEC forecasting uses 8 years (2008–2016) of GPS TEC data from

Manuscript received December 29, 2021; revised May 10, 2022; accepted June 1, 2022. Date of publication June 7, 2022; date of current version June 15, 2022. This work was supported in part by the Science and Engineering Research Board, Government of India, for ECRA File Ref. under Grant ECR/2018/001701 and in part by the Department of Science and Technology, New Delhi, India, for the FIST Program under Grant SR/FST/ET-II/2019/450. *(Corresponding author: Devanaboyina Venkata Ratnam.)*

The authors are with the Department of Electronics and Communication Engineering, Koneru Lakshmaiah Education Foundation, K L University, Guntur 522502, India (e-mail: sivakrishnakondaveeti@gmail.com; ratnam2002v@gmail.com; gsivavaraprasad@gmail.com).

Digital Object Identifier 10.1109/JSTARS.2022.3180940

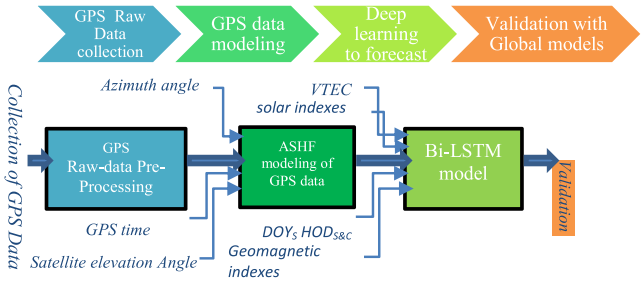

Fig. 1. Block diagram for ASHF-based bi-LSTM network.

the Bengaluru station (16.26°N, 80.44°E) [16]. The LSTM with convolutional NN (LSTM-CNN) model for ionospheric TEC forecasting uses GPS data taken over Bangalore station for eight years (2009–2016). The LSTM-CNN model has well captured the seasonal VTEC patterns [17]. However, the forecasting capability is limited to the local GNSS station only. The LSTM algorithm is implemented to forecast the spherical harmonics' coefficients and forecast the GIM [18]. Artificial neural-network-aided spherical cap harmonic analysis methodology is proposed for regional ionospheric mapping and studying the TEC maps over the Australian region [19]. Forecasting regional ionospheric TEC models are helpful to investigate the localized ionospheric disturbances. This article implements the ASHF-driven bi-LSTM TEC model with multivariate input parameters (solar and geomagnetic indices) to forecast ionospheric TEC maps over the Indian region. Bi-LSTMs train the network with two LSTMs instead of one. The first is on the input sequence, and the second is on a reversed copy of the input sequence, i.e., it utilizes both the past and future data for predictions [19]–[22].

A total of 64 ionospheric grid points (IGP) cover the entire Indian region with a spatial resolution of 5° × 5°. The ionospheric regional TEC forecasting maps are obtained from the Indian geographical latitude ranges from 5° N to 40° N and geographical longitude ranges from 65° E to 100° E. The real-time dual-frequency GPS TEC measurements are collected by the Indian GPS network of 26 GPS receivers. The nowcasting VTEC maps are generated using the derived ASHF coefficients. The ASHF-generated VTEC maps data are considered as input for the bi-LSTM algorithm. The forecasting of regional ionospheric TEC with a denser GPS receivers' network would provide ionospheric alerts to high-precision positioning and navigation applications, such as civil aviation and railways and automated driving.

The rest of this article is organized as follows. Section II of this article describes a detailed description of the proposed (bi-LSTM) algorithm. Section III describes the experimental results. Finally, Section IV concludes this article.

II. Proposed ASHF-Driven Bi-LSTM Model to Forecast Regional TEC Maps

The bi-LSTM-based TEC forecast model is implemented using ASHF modeled VTEC data obtained from 26 GPS stations, as shown in Fig. 1. The proposed DL model also requires knowledge of solar and geomagnetic parameters and ASHF-VTEC values to predict ionospheric TEC variations. Therefore, the input parameters, such as time, day, F10.7, and *Kp*, are considered input predictors. The stepwise details of the proposed approach are as follows.

Step 1: GPS measurements, such as week number, time (s), azimuthal angle(deg), elevation angle(deg), and STEC(TECu), with a 1-min time resolution are extracted from the Novatel GPS receivers of the model, GSV4000B for all 26 GPS stations.

Step 2: The conversion of slant TEC (STEC) into VTEC using a mapping function [3].

Step 3: The VTEC maps over 64 IGP are estimated using the ASHF nowcasting TEC model [3]. The GPS TEC maps are generated with a temporal resolution of 1-h step size.

Step 4: Preparation of hourly ASHF VTEC time series for each grid (total 64 grids) from 1 November 2015 to 31 October 2016.

The input parameters are considered as follows [23], [24].

Diurnal variation

HOD_s is the sine component of the universal hour number of the day. HOD_c is the cosine component of the universal hour number of the day.

$$HOD_s = \sin\left(\frac{2\pi \times hh}{24}\right) \tag{1}$$

$$HOD_c = \cos\left(\frac{2\pi \times hh}{24}\right). \tag{2}$$

Seasonal variation

DOY_s represent the sine component of numbering a day of the leap year. DOY_c represents the cosine component of numbering a day of the leap year.

$$DOY_s = \sin\left(\frac{2\pi \times dd}{366}\right) \text{leap year} \tag{3}$$

$$DOY_c = \cos\left(\frac{2\pi \times dd}{366}\right) \text{leap year} \tag{4}$$

where *dd* are the days in a year, and *hh* are the hours in a day.

The solar and geomagnetic parameters F10.7 and *Kp* are considered as input predictors.

The hourly ASHF VTEC values for each grid (total 64 grids) from 1 November 2015 to 31 October 2016 for 366 days are in terms of 8784 h for each IGP.

Step 5: Here, vtec_{IGP} is the TEC data extracted from ASHF modeling over Indian region.

$$[X]_{\text{grideddata(VTEC)}} = \begin{bmatrix} \text{vtec}_{\text{IGP1}} \\ : \\ : \\ : \\ \text{vtec}_{\text{IGP64}} \end{bmatrix}_{64\times 8784}. \tag{5}$$

X_{TRAIN} is the input predictor dataset that can be represented as follows:

$$X_{\text{TRAIN}} = \begin{bmatrix} \text{vtec}_{\text{IGP}}^{i} \\ HOD_{s}^{i} \\ HOD_{c}^{i} \\ DOY_{s}^{i} \\ DOY_{c}^{i} \\ F10.7^{i} \\ KP^{i} \end{bmatrix}_{7\times 8784} \tag{6}$$

$$X_1 = \begin{bmatrix} \text{vtec}_{\text{IGP}^1} \\ HOD_{s}^{1} \\ HOD_{c}^{1} \\ DOY_{s}^{1} \\ DOY_{c}^{1} \\ F10.7^{1} \\ KP^{1} \end{bmatrix}_{7\times 8784} \quad X_2 = \begin{bmatrix} \text{vtec}_{\text{IGP}^2} \\ HOD_{s}^{2} \\ HOD_{c}^{2} \\ DOY_{s}^{2} \\ DOY_{c}^{2} \\ F10.7^{2} \\ KP^{2} \end{bmatrix}_{7\times 8784}$$

$$X_{64} = \begin{bmatrix} \text{vtec}_{\text{IGP}^{64}} \\ HOD_{s}^{64} \\ HOD_{c}^{64} \\ DOY_{s}^{64} \\ DOY_{c}^{64} \\ F10.7^{64} \\ KP^{64} \end{bmatrix}_{7\times 8784}.$$

A. Bi-LSTM Methodology

Using bidirectional RNN possesses the inputs into two ways: one from past to future and another from future to past data. Moreover, this is different approach from LSTM unidirectional process. Adaptive moment estimation was used for optimization technique, which is gradient descend. The appropriate ionospheric features are extracted from raw data and provided as an input bi-LSTM network. Moreover, the input sequence of bi-LSTM also consists of the drivers for ionospheric responses, such as solar and geomagnetic activities, which fed to train two LSTM networks, as shown in Figs. 1 and 2. It combines LSTM and bi-directional RNN, which can handle information from both front and back [25]. This method has forward and backward connections and performs the training process in sequential order (see Fig. 2). The process inside the LSTMs in the proposed model is given below.

Let $i_t, o_t,$ and f_t are the input gate, the output gate, and the forget gate, respectively, at a time step t, where $t = 1$–24 h.

Bi-LSTM sequential forward:

$$i_t^f = \sigma\left(w_{xi}x_t + w_{hi}h_{t-1} + w_{ci}c_{t-1} + b_i\right) \tag{7}$$

$$f_t^f = \sigma\left(w_{xf}x_t + w_{hf}h_{t-1} + w_{cf}c_{t-1} + b_f\right) \tag{8}$$

$$c_t^f = f_t^f c_{t-1} + i_t \tanh\left(w_{xc}x_t + w_{hc}h_{t-1} + b_c\right) \tag{9}$$

$$o_t^f = \sigma\left(w_{x0}x_t + w_{h0}h_{t-1} + w_{co}c_t + b_0\right) \tag{10}$$

$$h_t^f = o_t \tanh\left(c_t^f\right). \tag{11}$$

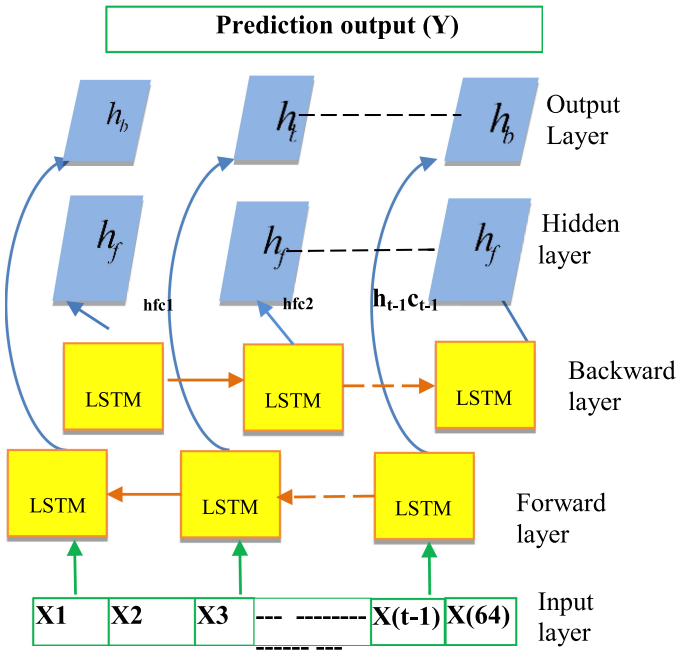

Fig. 2. Architecture for the bi-LSTM network.

Bi-LSTM sequential backward:

$$i_t^b = \sigma\left(w_{xi}x_t + w_{hi}h_{t+1} + w_{ci}c_{t+1} + b_i\right) \tag{12}$$

$$f_t^b = \sigma\left(w_{xf}x_t + w_{hf}h_{t+1} + w_{cf}c_{t+1} + b_f\right) \tag{13}$$

$$c_t^b = f_t^b c_{t+1} + i_t \tanh\left(w_{xc}x_t + w_{hc}h_{t+1} + b_c\right) \tag{14}$$

$$o_t^b = \sigma\left(w_{x0}x_t + w_{h0}h_{t+1} + w_{co}c_t + b_0\right) \tag{15}$$

$$h_t^b = o_t \tanh\left(c_t^b\right). \tag{16}$$

Step 1 at input gate: The input gate i_t of LSTM controls the flow of new information to the cell [13], [26], where h_{t-1} is the previous cell output, x_t is the current VTEC input vector, c_{t-1} is the previous cell memory, bias vector (b_i) and w_{xi}, w_{hi}, and w_{ci} are the weights of input vector, hidden state vector, and memory cell state at input gate, respectively.

Step 2 at forget gate: The forget gate f_t LSTM describes the amount of information from the previous internal state c_{t-1} that should be forgotten or stored [13]. The old memory (c_{t-1}), present input (x_t), previous output h_{t-1}, and bias vector can be merged by the pointwise summation operation and passes through the sigmoid function. The output of the sigmoid function is the value that is forgotten. The forget value can be varied between 0 and 1. Closer to 0 indicates to forget the information, and closer to 1 means to preserve the information.

Step 3 at updating the memory: In this step, it is required to decide the updated new information stores in the cell state. The memory of the current unit is given as [13], where w_{xc} and w_{hc} are the weights of input vector and hidden state vector of the cell state, respectively, and b_c is the bias vector.

Step 4 at output gate: Finally, the output(Y) for the LSTM unit is to be generated. This step provides the output valve that

TABLE I
BI-LSTM MODEL PARAMETERS

Parameters	Bi-LSTM
Learning method	DL
LSTM layers	2
LSTMcells	8784
Train Function	trainbr
Learning rate	0.005
Hidden units 1 no:	250
Hidden units 2 no:	250
length of sequence	8784
Optimizer	adam
Drop factor	0.2
mini batch Size	120
Maximum Epochs	3
Verbose	1
Loss function	MSE

is controlled by the input x_t, previous output h_{t-1}, updated memory c_t, and a bias vector b_0. The output is computed by bypassing the current input and the previous hidden state into a sigmoid function [13].

The one-hour ahead TEC value(Y) for each grid point value is repeated for 64 grid points all over the Indian region.

$$Y = \begin{bmatrix} \text{VTEC}^1 \\ \text{VTEC}^2 \\ \\ \text{VTEC}^{64} \end{bmatrix}_{64\times 1}. \tag{17}$$

The bi-LSTM feedforward network details are set in MATLAB, as given in Table I.

Table I presents the bi-LSTM parameters and hyperparameters considered. Improved forecasting results are obtained by adjusting the bi-LSTM model parameters. The adam optimizer is chosen for the optimization of the proposed forecasting method. The Train function "trainbr" is combined to optimize the parameters. The loss function is selected as MSE between the target TEC value and input TEC values.

B. Performance Analysis of the Proposed Bi-LSTM Model to Forecast Regional TEC Maps

Forecast performance is analyzed by Skill score1(SS1) and Skill score2 (SS2) and is known as the forecast score and forecast skill, respectively. The persistence is considered for the forecast performance of the proposed model. Here, one-hour persistence z_i^p is obtained from the model analysis z_i^o, and is expressed as

$$z_i^p = z_{i-1}^o. \tag{18}$$

The mean squared error (MSE) is the scalar accuracy measurement in forecast performance, where y_i^f is the ith forecast TEC value and z_i^o is the ith model TEC value, respectively.

Model MSE can be expressed as

$$\text{MSE}_{\text{model}} = \frac{1}{n}\sum_{i=1}^{n}\left(y_i^f - z_i^o\right)^2. \tag{19}$$

Here, n is the total number of observations in the proposed model.

Persistence MSE can be expressed as follows:

$$\text{MSE}_{\text{persist}} = \frac{1}{n}\sum_{i=1}^{n}\left(z_i^p - z_i^o\right)^2. \tag{20}$$

The MSE of the model and the average observed TEC are considered for computing the prediction efficiency (PE).

The PE is computed as follows:

$$\text{PE}_{\text{model}} = 1 - \frac{\text{MSE}_{\text{model}}}{\text{MSE}_{\text{model\_mean}}} \tag{21}$$

$$\text{PE}_{\text{persist}} = 1 - \frac{\text{MSE}_{\text{persist}}}{\text{MSE}_{\text{persisit\_mean}}}. \tag{22}$$

The Skill score 1 is defined as the ratio of PE of the model to that of persist of the PE.

The skill score 1 (SS1) can be calculated as

$$\text{SS1} = \frac{\text{PE}_{\text{model}}}{\text{PE}_{\text{persist}}}. \tag{23}$$

Forecast skill is a relative parameter obtained from forecast score as follows:

$$\text{SS2} = \frac{\text{PE}_{\text{persist}}(\text{SS1} - 1)}{1 - \text{PE}_{\text{persist}}}. \tag{24}$$

The skill score 1 or (forecast score) number should be greater than one for a better forecast performance, and the skill score 2 or (forecast skill) number should be greater than zero.

III. RESULTS AND DISCUSSION

The solar and geomagnetic indices are available in (https://omniweb.gsfc.nasa.gov/form/dx1.html).

The GPS TEC maps data are categorized into four seasons as summer (May–August), winter (January–February 2016 and November–December 2015), autumn equinox (September–October), and vernal equinox (March–April). The training data of 261 days (November 2015 to September 2016) are given as input to the bi-LSTM ionospheric forecasting algorithm. The validation dataset for 24 days in September 2016 and testing data for 31 days in October 2016 are considered to evaluate the performance of bi-LSTM model forecasting accuracy. Fig. 3 shows a typical ionospheric TEC variability for IGP location (80°E, 15°N). Fig. 3 shows that diurnal ionospheric behavior and a maximum TEC of 60 TECU are noticed during the March month. It is observed that March equinox ionospheric TEC values are higher than Autumn equinox, confirming seasonal asymmetry (see Fig. 3). Seasonal asymmetry is mainly due to the changes in the ratio of concentrations of atomic oxygen and molecular nitrogen [27]. The F10.7 solar index and sunspot

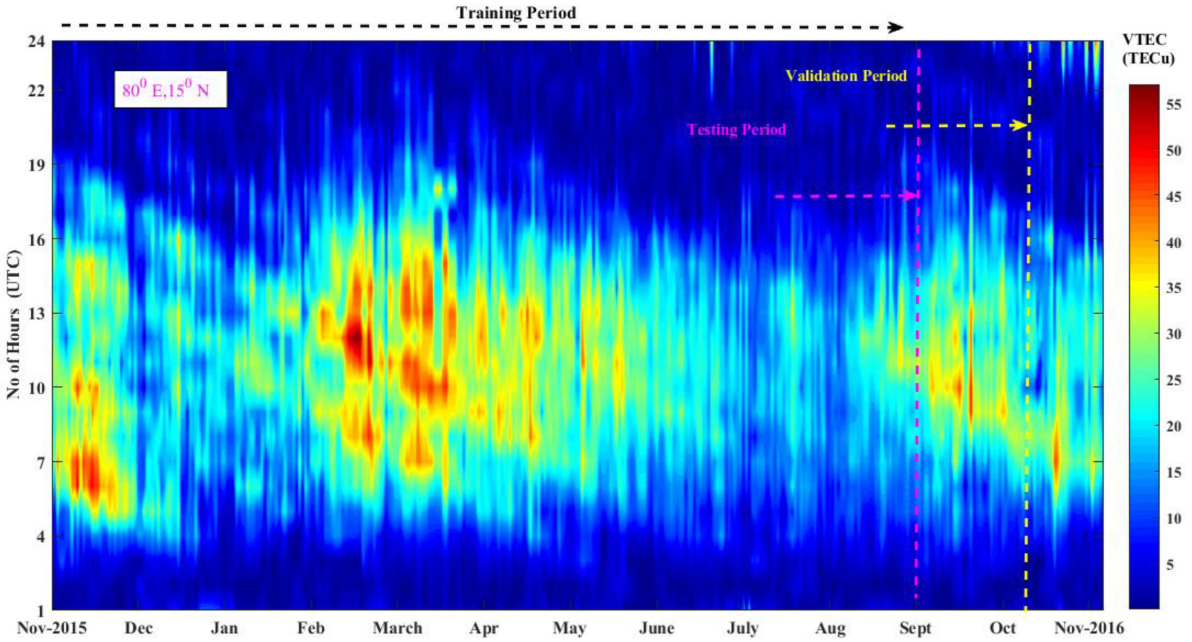

Fig. 3. Typical GPS VTEC at GP 80°E, 15°N to monitor ionospheric TEC variations using ASHF model (similarly for all 26 GPS TEC stations data).

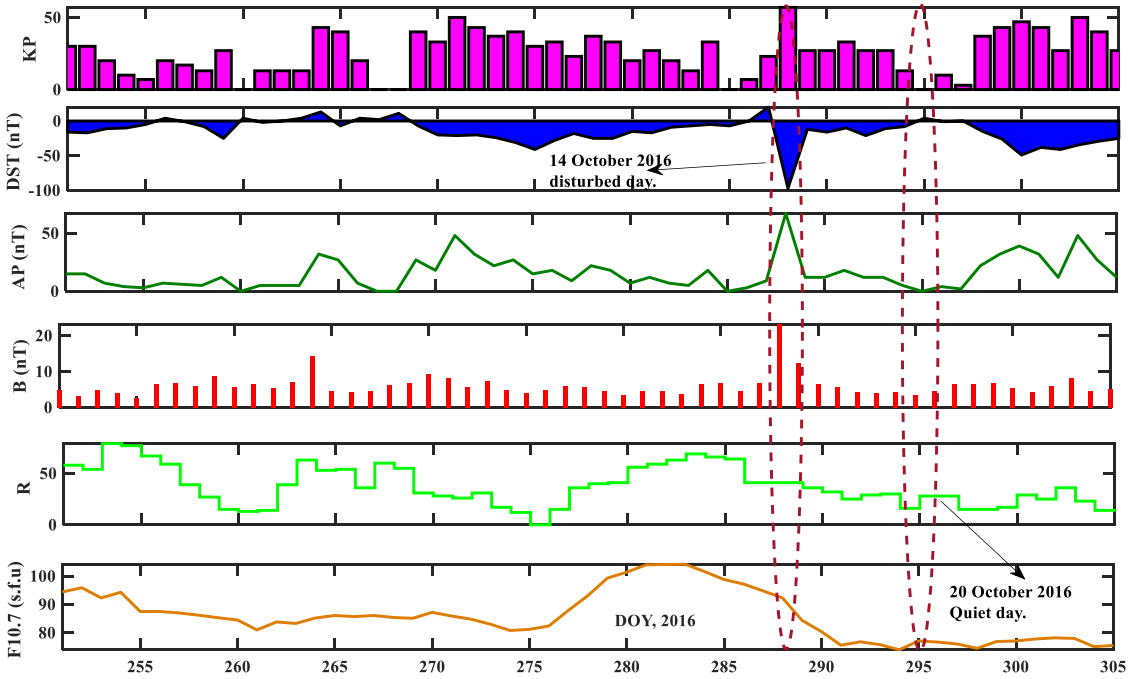

Fig. 4. Solar and geomagnetic indices variations during the testing period (7 September 2016 to 31 October 2016).

number variations are shown in the bottom panel of Fig. 4. The F10.7 solar index was almost the high (90sfu), and the sunspot number is also high on 14 October 2016. The minimum F10.7 (74sfu) and sunspot R values are noticed on 20th October 2016. The geomagnetic indices are $Kp*10$ Index, Dst Index, (nT), Ap index, and solar wind B(nT), whose values are shown in the top panel of Fig. 4. The maximum Kp index value of 55 was on 14 October 2016. It can be seen that the Dst. Index sharply increased from ∼55 to ∼110 nT (see Fig. 4). The Ap index also increased from ∼10 to ∼65 nT on 14 October, and from Fig. 4, the Ap dropped to ∼0 on 20th October 2016. The maximum solar wind B(nT) is 22 nT on 14 October 2016, and the minimum B (nT) value of 5 nT is noticed on 20 October 2016, considering the solar and geomagnetic indices properties.

Fig. 5(a) shows b quiet day variations of different ionospheric forecasting models on 20 October 2016. The proposed

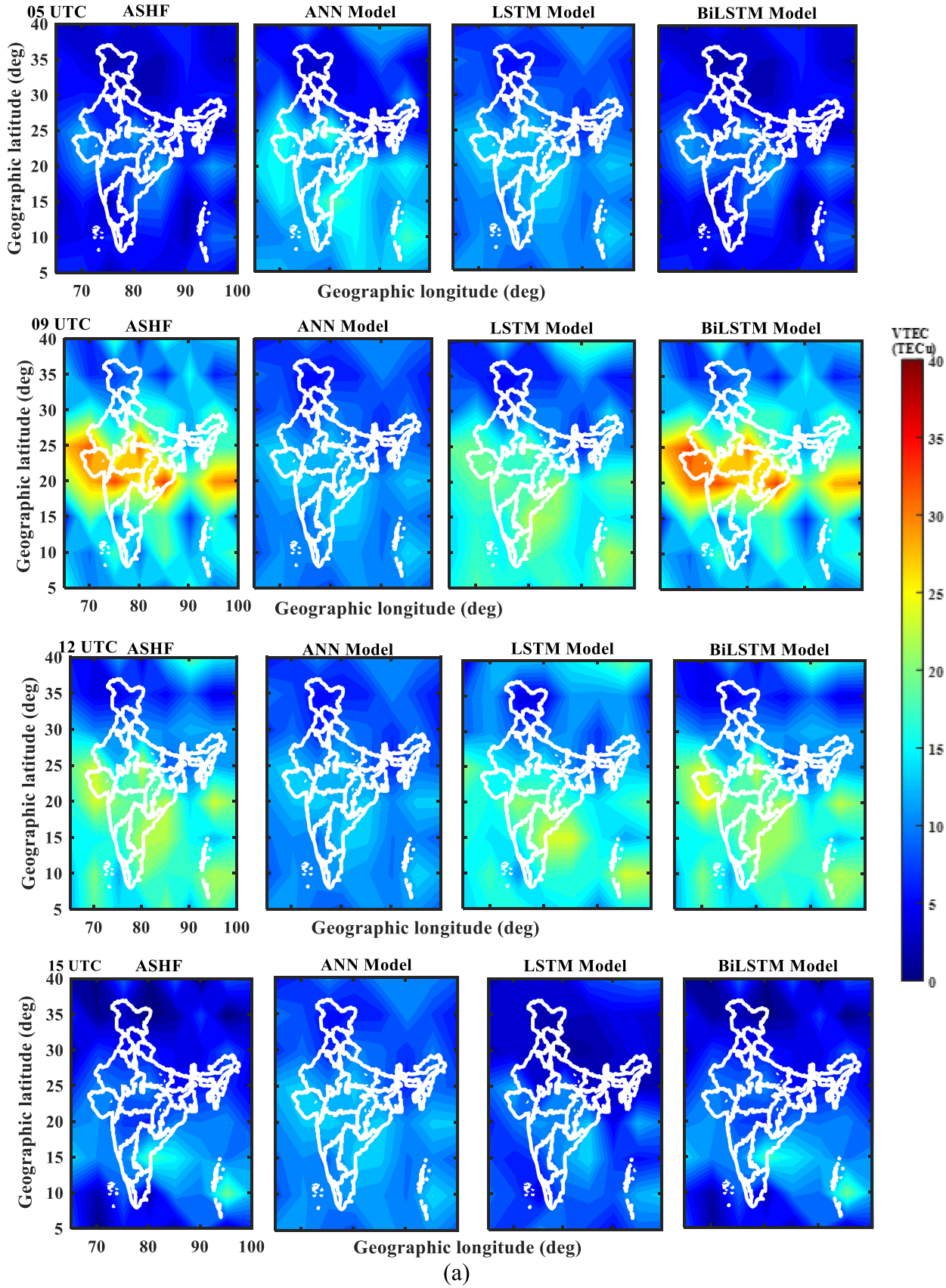

(a)

Fig. 5. (a) ASHF, ANN, LSTM, and bi-LSTM spatial TEC variations models during geomagnetic quiet day, 20 October 2016. (b) TEC bias estimated among ASHF, ANN, LSTM, and bi-LSTM models during geomagnetic quiet day, 20 October 2016.

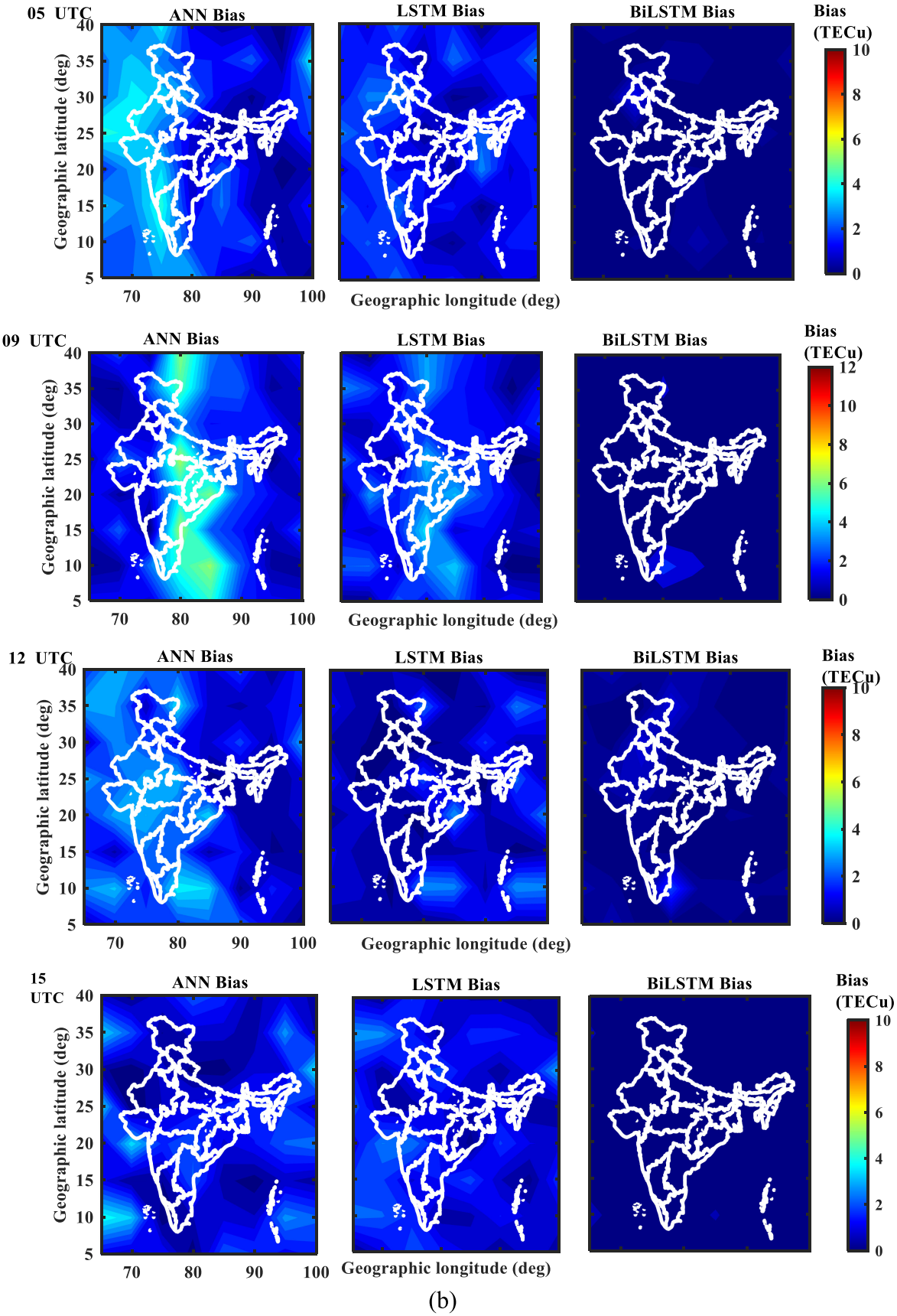

(b)

Fig. 5. (Continued.)

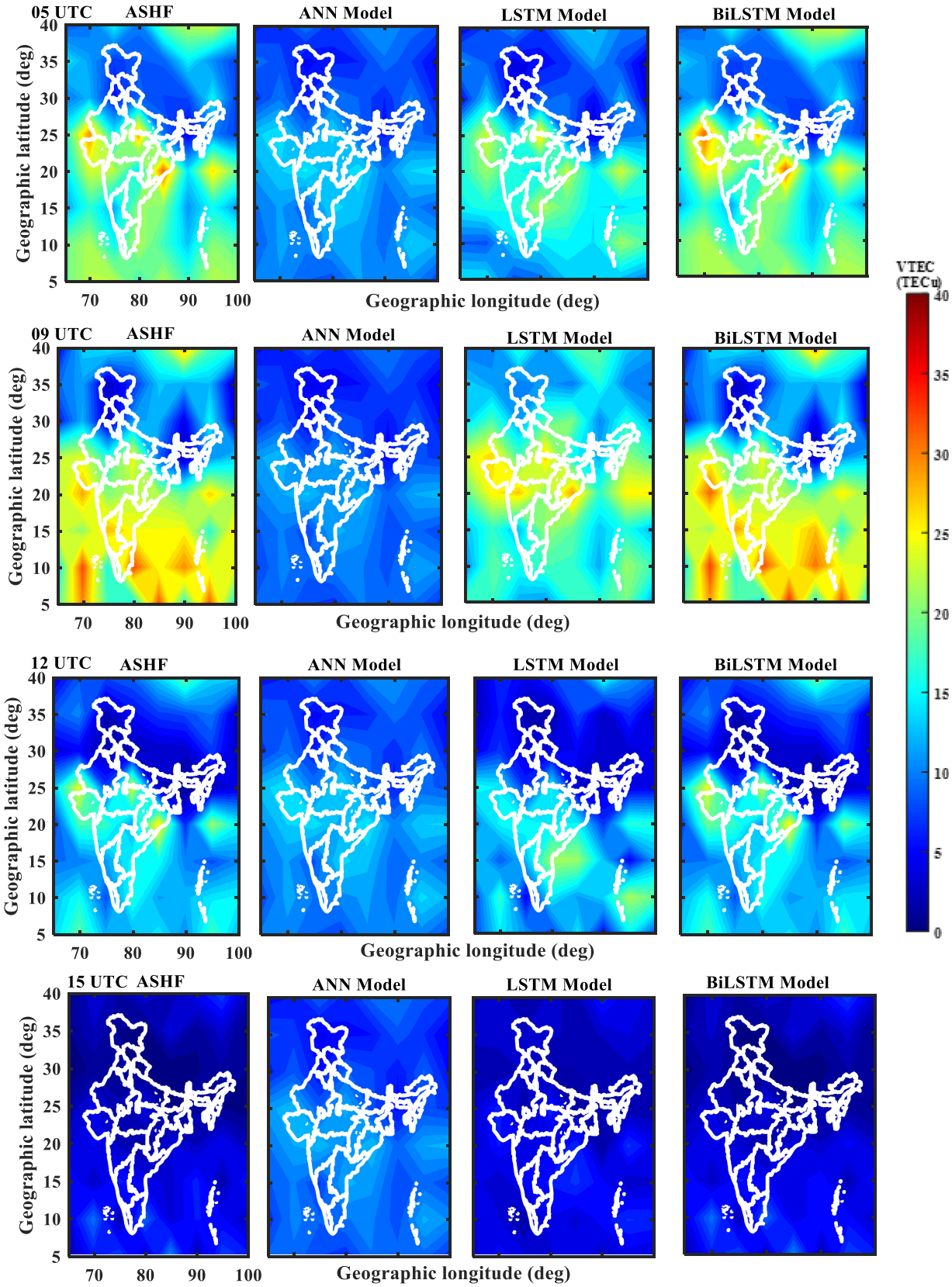

Fig. 6. (a) ASHF, ANN, LSTM, and bi-LSTM TEC models for geomagnetic disturbed day (14 October 2016). (b) TEC bias estimated among ASHF, ANN, LSTM, and bi-LSTM models during geomagnetic for disturbed day (14 October 2016).

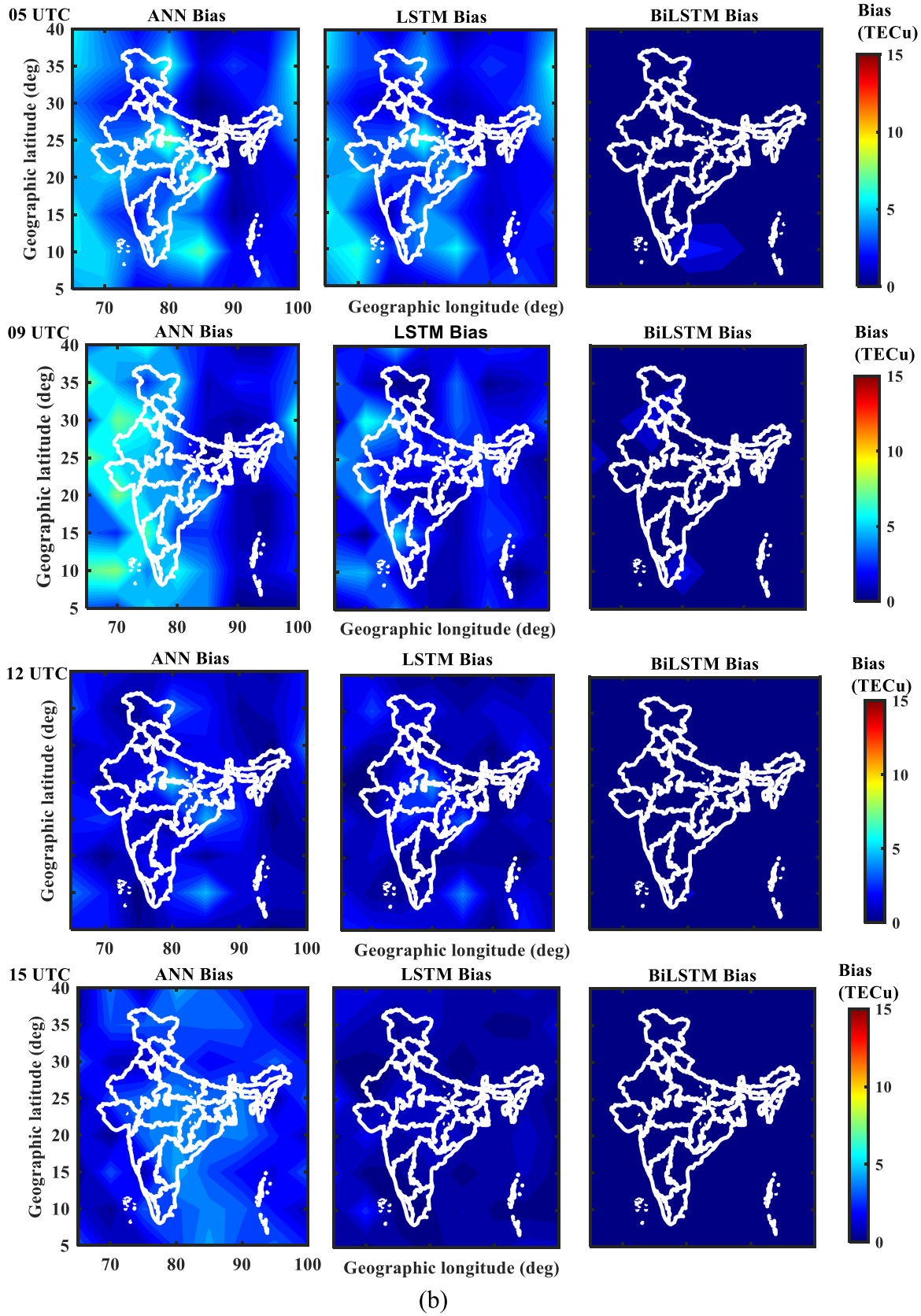

(b)

Fig. 6. (Continued.)

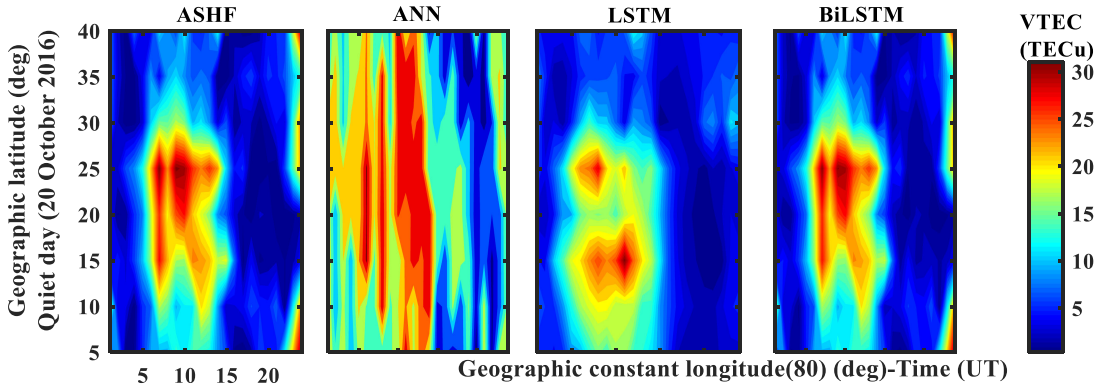

Fig. 7. Temporal EIA variations observed over 80° E longitude for geomagnetic quiet day, 20 October 2016.

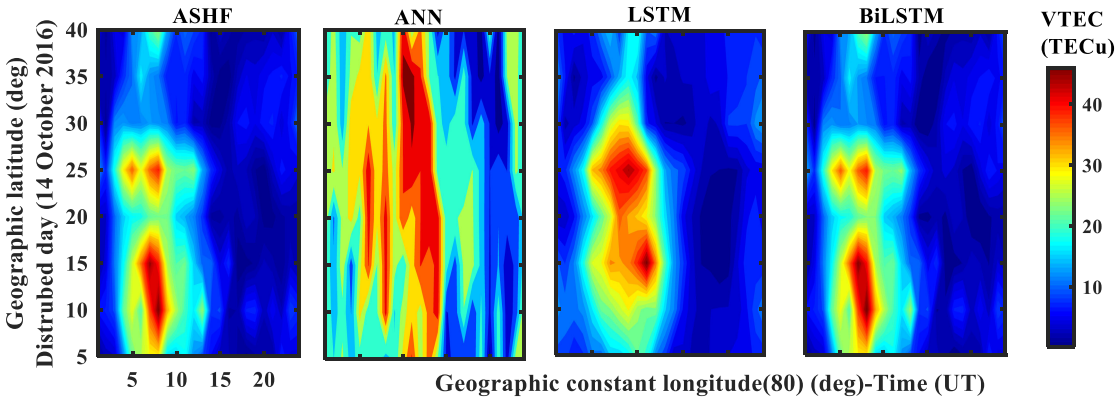

Fig. 8. Temporal EIA variations observed over 80° E longitude for the geomagnetic disturbed day (14 October 2016).

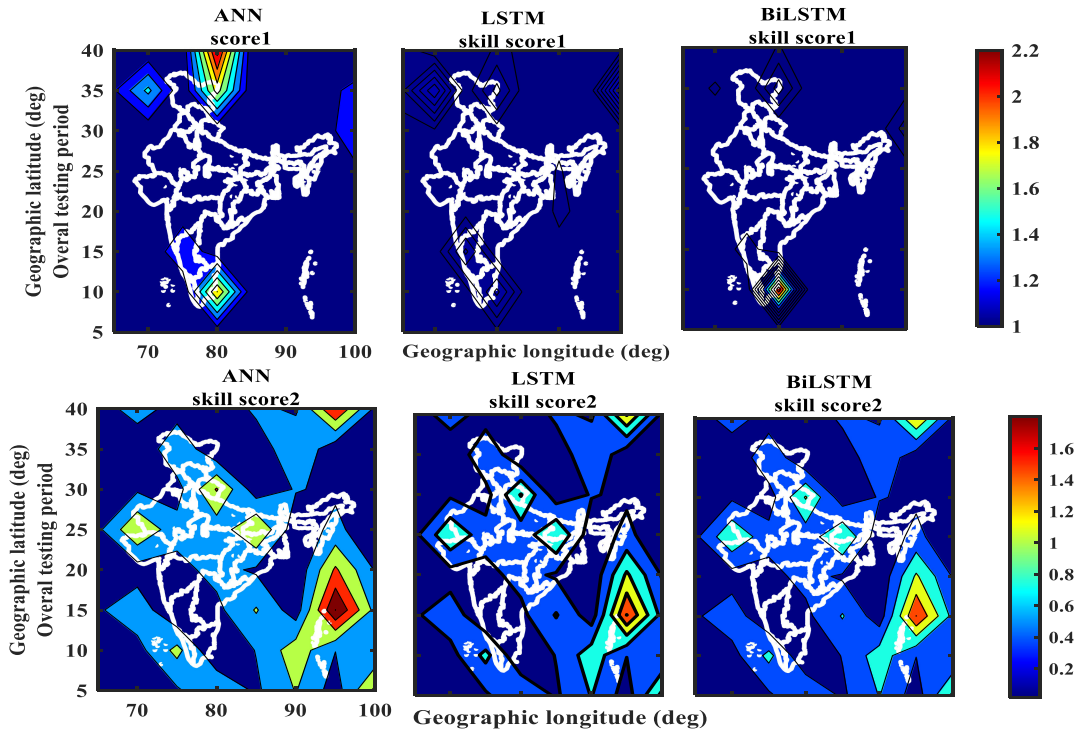

Fig. 9. Skill scores of bi-LSTM, ANN, and LSTM models overall testing period.

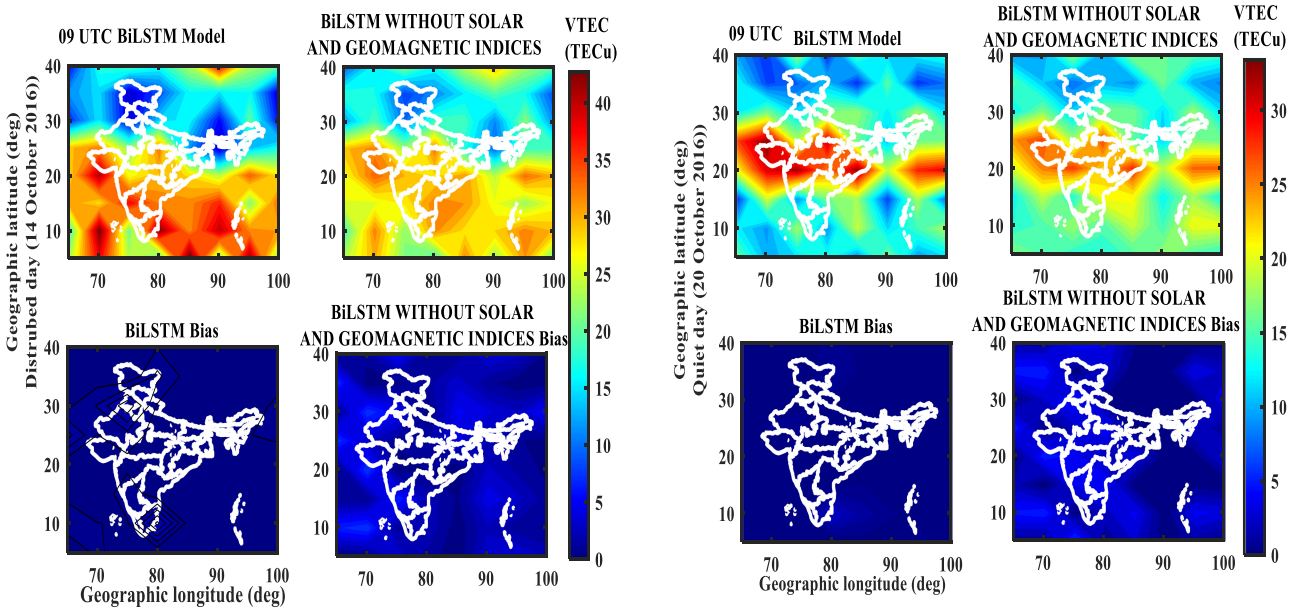

Fig. 10. Comparison of ionospheric forecasting results between with and without solar and geomagnetic indices as input to bi-LSTM, during quiet day, 20 October 2016, and disturbed days (14 October 2016), at 09:00 UTC hours.

bi-LSTM model predicted the TEC structure entry compared with the observed TEC structures. The fully developed TEC occupancy was observed at 09:00 and 12.00 hrs UTC at the northwestern part of India with the maximum TEC of 27 TECU (09.00 hrs UTC) and 23 TECU (12.00 hrs UTC). However, LSTM model has predicted better TEC values than the ANN models during 05.00UTC to 15.00 UTC hours. Bi-LSTM model has forecasted the occurrence of EIA patterns as seen from the time instant from 05.00 to 15.00 UTC hrs. The exit of EIA movement is observed at 15.00 hrs UTC with a maximum VTECU of 20TECu. The bi-LSTM model well forecasts the movement of exit EIA TEC structures compared with the other models for quiet day conditions.

Fig. 5(b) shows the absolute difference of ANN, LSTM models, and proposed regional bi-LSTM maps' values with observed TEC values during the quiet day, 20 October 2016. It is observed that the bi-LSTM results show the lowest TEC bias values compared with the other models at 05:00 UTC. The difference of TEC bias values varies between 1 TECU to 2.5 TECU. However, the LSTM model has performed better than the ANN model with a maximum bias of 4 TECU. Nevertheless, to say that bi-LSTM model bias TEC values are lower than the other models with a maximum of 2 TECU occurred at IGP location 15° N and 90° E and 2.5TECu at 35° N and 80° E during 15:00 UTC hours, correspondingly.

The ionospheric forecasting model TEC results for the disturbed day (14 October 2020) are shown in Fig. 6(a). The entry of EIA phenomena is noticed at 5.00 hrs UTC with a maximum of TEC of 20 TECU in the central part of India. The depleted EIA is passing over the southern part of Indian near to crest and is observed at 09.00 hrs TEC with a maximum TEC of 34TECU using the ASHF model. The bi-LSTM model predicted the fully EIA occupancy during 09:00 hrs UTC. The ANN and LSTM models have overestimated the TEC values compared with the ASHF TEC values.

Fig. 6(b) shows the absolute difference of ANN, LSTM model, and the proposed regional bi-LSTM TEC maps for the geomagnetically disturbed day (14 October 2016). It is observed that the bi-LSTM model yields low forecasting bias (1 TECU to 3.5 TECU) compared with ANN and LSTM models. However, the biases of LSTM and ANN models are varied up to 15 TECU at 05:00 UTC hours, 09:00 UTC hours, 12:00 UTC hours, and 15:00 UTC hours, respectively. Also, the LSTM model performs better than the ANN model with maximum bias TEC values of 4 TECU. It is evident that the maximum bias values of the bi-LSTM model are 3 TECU at IGP (15° N and 90° E) during 05:00 UTC hours and 2.5 TECU at IGP (35° N and 80° E) during 15:00 UTC hours, respectively.

The northern crest EIA variations for Indian latitudes over meridional cross section at 80° E longitude for a quiet day (20 October 2016) is shown in Fig. 7. The LSTM model estimated the northern EIA from the crest to trough at 10:00 hrs UTC. Bi-LSTM predicted the maximum TEC (45TEC) at 25° latitudinal bands indicating the regular formation of northern EIA structure for quiet day conditions. Fig. 8 gives the temporal EIA variations of ANN, LSTM, and bi-LSTM forecasting results for the geomagnetically disturbed day. All the models captured the early movement of EIA that occurred at 09.00 hrs UTC. However, the bi-LSTM model has predicted EIA TEC structures depleted and downward shift compared with the ASHF model. Fig. 9 shows the Skill scores of bi-LSTM, ANN, and LSTM models overall testing period.

From Fig. 9, it is evident that all modes forecasting skill scores 1 is greater than 1 and forecasting skill scores 2 is greater than 0. The bi-LSTM model skill scores 1 and 2 are the low values of 1.3 and 1.7. The forecasting skill results reveal that the bi-LSTM

forecasting model has improved predicting the TEC response compared with the other selected ionospheric models.

Fig. 10 shows a comparison between the Indian regional ionospheric forecast TEC maps with and without solar and geomagnetic indices as input to bi-LSTM, during quiet day, (20 October 2016) and disturbed days (14 October 2016) at 09:00 UTC hours. The regional ionospheric forecast TEC maps with solar and geomagnetic indices as input to bi-LSTM can be slightly better than without solar and geomagnetic indices as input to bi-LSTM.

IV. Conclusion

A DL algorithm based on bi-LSTM is performed for forecasting ionospheric TEC values over the Indian region using 26 dense GPS station network data. The gridded TEC time-series dataset is analyzed from November 2015 to October 2016 with one-hour ahead of forecasting. The long-term data from November 2015 to September 2016 over the Indian region are used to implement and test the performance of the proposed model. The two LSTMs for forward and backward connection pass the spatial and temporal information, leading to improved bi-LSTM compared with the ANN and LSTM models. The bi-LSTM model well predicts the quiet time regular northern EIA TEC structures and is reasonably predicted by ANN and LSTM. Furthermore, the bi-LSTM model can capture the downward shift of depleted EIA TEC structures on geomagnetically disturbed conditions. The regional ionospheric forecast TEC maps with solar and geomagnetic indices as input to bi-LSTM are slightly better than without the solar and geomagnetic indices as input to bi-LSTM. The preliminary results confirm that the bi-LSTM model improves efficiency by exploring both the past and future information. The data patches in terms of artifacts are noticed over the Indian region and may be due to the data sparsity and low-order ASHF model limitations. The data sparsity and ASHF model limitations will be handled by employing an assimilation or ML approach. In the future, the present work will be extended to develop a DL-aided web-based ionospheric forecasting system for GNSS users.

References

[1] S. Raghunath and D. V. Ratnam, "Ionospheric spatial gradient detector based on GLRT using GNSS observations," *IEEE Geosci. Remote Sens. Lett.*, vol. 13, no. 6, pp. 875–879, Jun. 2016.

[2] C. M. Ho, B. D. Wilson, A. J. Mannucci, U. J. Lindqwister, and D. N. Yuan, "A comparative study of ionospheric total electron content measurements using global ionospheric maps of GPS, TOPEX radar, and the Bent model," *Radio Sci.*, vol. 32, no. 4, pp. 1499–1512, Jul./Aug. 1997.

[3] K. S. Krishna, D. V. Ratnam, M. Sridhar, P. B. S. Harsha, and G. Sivavaraprasad, "Performance evaluation of adjusted spherical harmonics ionospheric model over Indian region," *IEEE Access*, vol. 8, pp. 172610–172622, 2020.

[4] D. Chunli and P. Jinsong, "Modeling and prediction of TEC in China region for satellite navigation," in *Proc. 15th Asia-Pacific Conf. Commun.*, 2009, pp. 310–313.

[5] X. Li and D. Guo, "Modeling and prediction of ionospheric total electron content by time series analysis," in *Proc. 2nd Int. Conf. Adv. Comput. Control*, 2010, pp. 375–379.

[6] R. Niu, C. Guo, Y. Zhang, L. He, and Y. Mao, "Study of ionospheric TEC short-term forecast model based on combination method," in *Proc. 12th Int. Conf. Signal Process.*, 2014, pp. 2426–2430.

[7] E. O. Oyeyemi, L. A. McKinnell, and A. W. V. Poole, "Near-real time foF2 predictions using neural networks," *J. Atmos. Sol.-Terr. Phys.*, vol. 68, pp. 1807–1818, 2006.

[8] S. Lee, E.-Y. Ji, Y.-J. Moon, and E. Park, "One-day forecasting of global TEC using a novel deep learning model," *Space Weather*, vol. 19, 2021, Art. no. e2020SW002600.

[9] S. Asaly, L.-A. Gottlieb, and Y. Reuveni, "Using support vector machine (SVM) and ionospheric total electron content (TEC) data for solar flare predictions," *IEEE J. Sel. Topics Appl. Earth Observ. Remote Sens.*, vol. 14, pp. 1469–1481, 2021.

[10] A. V. Zhukov, Y. V. Yasyukevich, and A. E. Bykov, "GIMLi: Global ionospheric total electron content model based on machine learning," *GPS Solutions*, vol. 25, 2021, Art. no. 19.

[11] E. Tulunay, E. T. Senalp, S. M. Radicella, and Y. Tulunay, "Forecasting total electron content maps by neural network technique," *Radio Sci.*, vol. 41, no. 4, pp. 1–12, Aug. 2006.

[12] Z. Huang and H. Yuan, "Ionospheric single-station TEC short-term forecast using RBF neural network," *Radio Sci.*, vol. 49, no. 4, pp. 283–292, Apr. 2014.

[13] T. Yuan, Y. Chen, S. Liu, and J. Gong, "Prediction model for ionospheric total electron content based on deep learning recurrent neural networkormalsize," *Chin. J. Space Sci.*, vol. 38, no. 1, pp. 48–57, 2018.

[14] W. Sun *et al.*, "Forecasting of ionospheric vertical total electron content (TEC) using LSTM networks," in *Proc. Int. Conf. Mach. Learn. Cybern.*, 2017, pp. 340–344.

[15] P. Xiong, D. Zhai, C. Long, H. Zhou, X. Zhang, and X. Shen, "Long short-term memory neural network for ionospheric total electron content forecasting over China," *Space Weather*, vol. 19, 2021, Art. no. e2020SW002706.

[16] I. Srivani, G. Siva Vara Prasad, and D. Venkata Ratnam, "A deep learning-based approach to forecast ionospheric delays for GPS signals," *IEEE Geosci. Remote Sens. Lett.*, vol. 16, no. 8, pp. 1180–1184, Aug. 2019.

[17] A. Ruwali, A. J. Sravan Kumar, K. B. Prakash, G. Sivavaraprasad, and D. Venkata Ratnam, "Implementation of hybrid deep learning model (LSTM-CNN) for ionospheric TEC forecasting using GPS data," *IEEE Geosci. Remote Sens. Lett.*, vol. 18, no. 6, pp. 1004–1008, Jun. 2021.

[18] L. Liu, S. Zou, Y. Yao, and Z. Wang, "Forecasting global ionospheric TEC using deep learning approach," *Space Weather*, vol. 18, no. 11, 2020, Art. no. e2020SW002501.

[19] W. Li, D. Zhao, Y. Shen, and K. Zhang, "Modeling Australian TEC maps using long-term observations of Australian regional GPS network by artificial neural network-aided spherical cap harmonic analysis approach," *Remote Sens.*, vol. 12, no. 23, 2020, Art. no. 3851.

[20] O. Zennaki, N. Semmar, and L. Besacier, "Inducing multilingual text analysis tools using bidirectional recurrent neural networks," 2016, *arXiv:1609.09382*.

[21] Y. Bin, Y. Yang, F. Shen, X. Xu, and H. T. Shen, "Bidirectional long-short term memory for video description," in *Proc. 24th ACM Int. Conf. Multimedia*, 2016, pp. 436–440.

[22] W. Sun, L. Xu, X. Huang, W. Zhang, T. Yuan, and Y. Yan, "Bidirectional LSTM for ionospheric vertical total electron content (TEC) forecasting," in *Proc. IEEE Vis. Commun. Image Process.*, 2017, pp. 1–4.

[23] D. Okoh *et al.*, "A neural network-based ionospheric model over Africa from constellation observing system for meteorology, ionosphere, and climate and ground global positioning system observations," *J. Geophysical Res.: Space Phys.*, vol. 124, no. 12, pp. 10512–10532, 2019.

[24] J. B. Habarulema *et al.*, "A global 3-D electron density reconstruction model based on radio occultation data and neural networks," *J. Atmos. Sol.-Terr. Phys.*, vol. 221, 2021, Art. no. 105702.

[25] A. Hu and K. Zhang, "Using bidirectional long short-term memory method for the height of F2 peak forecasting from ionosonde measurements in the Australian region," *Remote Sens.,* vol. 10, 2018, Art. no. 1658.

[26] T. V. Rao, M. Sridhar, D. Venkata Ratnam, P. B. S. Harsha, and I. Srivani, "A bidirectional long short-term memory-based ionospheric foF2 and hmF2 models for a single station in the low latitude region," *IEEE Geosci. Remote Sens. Lett.*, vol. 19, 2022, Art. no. 8005405.

[27] H. Rishbeth and C. S. G. K. Setty, "The F-layer at sunrise," *J. Atmos. Terr. Phys.*, vol. 20, no. 4, pp. 263–276, Apr. 1961.

[28] M. Kaselimi, A. Voulodimos, N. Doulamis, A. Doulamis, and D. Delikaraoglou, "A causal long short-term memory sequence to sequence model for TEC prediction using GNSS observations," *Remote Sens.*, vol. 12, no. 9, 2020, Art. no. 1354.

Kondaveeti Sivakrishna received the M.tech. degree in digital electronics and communication systems from Samuel Gerorge Institute of Engineering and Technology College, Andhra Pradesh, Jawaharlal Nehru Technological University Hyderabad, Hyderabad, India, in 2012.

He is working as a Senior Research Fellow, SERB ECR/2018/001701 Project and Research Scholar, with Space Technology and Atmospheric Research Laboratory, Department of Electronics and Communication Engineering, Koneru Lakshmaiah Education Foundation, Guntur, India. His research interests include ionospheric TEC modeling and study of ionospheric single-frequency GPS receivers, developing algorithms of DCBs. At present, his research is focused on the development of machine learning algorithms for GNSS/NavIC observations. He has authored or coauthored more than six SCI papers, including IEEE journals.

Devanaboyina Venkata Ratnam (Senior Member, IEEE) received the M.tech. degree in radar and microwave engineering from the Department of Electronics and Communication Engineering, Andhra University, Visakhapatnam, India, in 2003, and the Ph.D. degree in electronics and communication engineering from Jawaharlal Nehru Technological University Hyderabad, Hyderabad, India, in 2011.

From 2003 to 2011, he worked as a Research Assistant, Junior Research Fellow, Senior Research Fellow, and Senior Research Assistant with the Research and Training Unit for Navigational Electronics, Osmania University, Hyderabad, India. In 2011, he joined as an Associate Professor with the Faculty of Department of Electronics and Communications Engineering and is currently working as a Professor and Head Research of the Department of Electronics and Commuication Engineering and the Head of the Centre for Atmospheric Sciences, K L University, Guntur, India. His research interests include navigational electronics, global navigational satellite systems, space science, and radio-wave propagation. He has authored or coauthored more than 66 journal papers.

Dr. Ratnam was the recipient of the Young Scientist Award (2012–2015) of the Department of Science and Technology, India, and the Research Award (2015–2017) of the University Grants Commission, India, and Early Career Research Award (2017–2020) from Science and Engineering Research Board, India.

Gampala Sivavaraprasad (Member, IEEE) received the M.tech. degree in communications and radar systems from K L University, Guntur, India, in 2015, and the Ph.D. degree in satellite communication and navigation systems from the Department of Electronics and Communication Engineering (ECE), K L University, Guntur, India, in 2018.

In 2017, he joined as an Assistant Professor with the Faculty of Department of ECE, K L University, where he is currently working as an Assistant Professor. He is a premier professional member of the Institute of Navigation. His research interests include satellite and wireless communication systems, space weather studies of upper atmosphere, study of ionospheric irregularities using GPS-based TEC, and scintillations' measurements. His current research is focused on the development of web-based ionospheric system based on deep learning techniques for ionospheric total electron content forecasting and mitigation of scintillation effects using GNSS/NavIC observations. He has authored or coauthored more than 15 SCI papers, including IEEE journals.

Dr. Sivavaraprasad was a recipient of the Early Career Research Award from Science and Engineering Research Board, India, from 2019 to 2022.